frontiers | Frontiers in Astronomy and Space Sciences

TYPE Original Research
PUBLISHED 03 January 2024
DOI 10.3389/fspas.2023.1233060

OPEN ACCESS

EDITED BY
John C. Dorelli,
National Aeronautics and Space Administration, United States

REVIEWED BY
Kristina A. Lynch,
Dartmouth College, United States
Shishir Priyadarshi,
GMV NSL, United Kingdom

*CORRESPONDENCE
G. J. Fasel,
gfasel@pepperdine.edu

RECEIVED 01 June 2023
ACCEPTED 14 November 2023
PUBLISHED 03 January 2024

CITATION
Fasel GJ, Lee LC, Lake E, Csonge D, Yonano B, Bradley O, Briggs J, Lee SH, Mann J, Sigernes F and Lorentzen D (2024), Correlation between the solar wind speed and the passage of poleward-moving auroral forms into the polar cap.
Front. Astron. Space Sci. 10:1233060.
doi: 10.3389/fspas.2023.1233060

Correlation between the solar wind speed and the passage of poleward-moving auroral forms into the polar cap

G. J. Fasel[1]*, L. C. Lee[2], E. Lake[1], D. Csonge[1], B. Yonano[1], O. Bradley[1], J. Briggs[1], S. H. Lee[3], J. Mann[1], F. Sigernes[4] and D. Lorentzen[4]

[1]Natural Science Department, Pepperdine University, Malibu, CA, United States, [2]Institute of Earth Sciences, Academia Sinica, Taipei City, Taiwan, [3]NASA Goddard Space Flight Center, Greenbelt, MD, United States, [4]Geophysical Department, University Centre in Svalbard, Longyearbyen, Norway

In 1961, Dungey suggested that magnetic reconnection occurs due to the solar-terrestrial interaction. The interplanetary magnetic field (IMF) is thought to merge with Earth's geomagnetic field (GMF). After the reconnection process the newly formed magnetic flux tube, consisting of both the IMF and GMF, moves anti-sunward. Poleward-moving auroral forms (PMAFs) are believed to be the ionospheric signatures of this process, which transfers magnetic flux from the dayside to the nightside. This paper looks at the connection between the solar wind speed and the motion of the PMAF as it moves from the auroral oval, anti-sunward, into the polar cap. PMAFs are identified using both the meridian scanning photometer (MSP) and colored all-sky camera (ASC). Once the PMAFs are identified, the PMAF-SLOPE, v_α (units of degrees per time) and the angle (α_{PMAF}) the PMAF makes with the horizontal (Time axis), in the MSP plot are calculated. These values (v_α and α_{PMAF}) are individually plotted against the v_x-component of the solar wind speed and the flow speed (total solar wind speed). The plots generate linear a relationship between PMAF-SLOPEs, v_α, [or PMAF angles (α_{PMAF})], and the v_x-component of the solar wind speed (or the flow speed). A total of 57 PMAF events from 8 different days were associated with solar wind speeds (v_x-component) ranging from 344 to 679 km/s. The first linear plot, between the PMAF-SLOPE and solar wind speed (v_x-component), shows a high correlation: $r_{v_\alpha} = 0.944$. A second linear plot, between α_{PMAF} and the solar wind speed (v_x-component) shows a very high correlation: $r_{\alpha PMAF} = 0.973$. The conclusions obtained from this statistical study are: 1) both the PMAF-SLOPE v_α and α_{PMAF} are highly correlated to the v_x-component of the solar wind, increasing when v_x increases and *vice versa*, 2) PMAFs must be connected to both the IMF and GMF and are dragged anti-sunward, mostly by the v_x-component of the solar wind, and 3) PMAFs are indeed the ionospheric footprints of a newly formed magnetic flux tube, due to dayside magnetic reconnection, being transferred from the dayside to nightside.

KEYWORDS

magnetosphere, reconnection, solar wind, ionosphere, transients

1 Introduction

The solar-terrestrial interaction provides an astrophysical laboratory to study how a star interacts with a magnetized planet. During this interaction, magnetic flux is transferred from the dayside to the nightside via magnetic reconnection when the interplanetary magnetic field (IMF) merges with a geomagnetic field (GMF) on the dayside magnetopause. As the IMF moves anti-sunward, it drags the newly formed flux tube (IMF + GMF) towards the nightside.

Dungey (1961) first suggested that magnetic reconnection takes place at two magnetic neutral lines: one at the sub-solar magnetopause and the other in the geomagnetic tail. This process is now believed to be the main mechanism for the transfer of solar wind momentum and energy into the magnetosphere. High latitude satellite observations were first used to identify magnetic reconnection at the dayside magnetopause (Haerendel et al., 1978; Russell and Elphic, 1978). Haerendel et al. (1978) used HEOS 2 observations to conclude that reconnection could be an "intermittent, localized process which does not lead to the buildup of a regular boundary flow". Russell and Elphic [1979]; CT Russell and Elphic [1978] using USEE 1 and 2 magnetometer data identified flux transfer events (FTEs). Statistical studies (Berchem and Russell, 1984; Daly et al., 1984; Paschmann et al., 1982; Rijnbeek et al., 1984; Saunders et al., 1984) of FTEs have borne out observed signatures, spatial location of occurrences, and the relation of solar wind parameters for these reconnection events. The above mentioned studies of FTEs show that they 1) are spatially localized, (Russell and Elphic, 1979), 2) are of short time duration, (Russell and Elphic, 1979), 3) have a bipolar signature of the magnetic normal component normal to the magnetopause, B_n, (Daly et al., 1984; Rijnbeek et al., 1984; Russell and Elphic, 1979), 4) sometimes have a twisted core magnetic field (Saunders et al., 1984), 5) are on the order of one Earth radius in the direction normal to the magnetopause (Rijnbeek et al., 1984; Saunders et al., 1984), 6) have a mixture of magnetospheric and magnetosheath plasmas (Paschmann et al., 1982), 7) have an average of ≈8 min between events (Lockwood and Wild, 1993; Rijnbeek et al., 1984), 8) occur mainly when the IMF B_z-component is southward, but there have been very few events observed when the IMF B_z is northward (Berchem and Russell, 1984).

During the southward turning of the IMF B_z-component the merging rate on the dayside increases (Newell and Meng, 1987) leading to the erosion of the dayside magnetopause. Aubry et al. (1970) reported inward motion of the magnetopause of ≈2R_E in 2 h from Ogo 5 satellite observations. This inward motion of the magnetopause is associated with a change in the IMF B_z-component, from $B_z>0$ to $B_z<0$, and since the inward movement is not associated with a compression of the magnetospheric cavity, they concluded that magnetic flux was being transferred from the dayside magnetopause to the magnetotail (Aubry et al., 1970). *Meng* [1970] also reported the inward movement of the dayside magnetopause from its nominal position, from IMP 2 data, during the occurrences of polar substorms.

Measurements of the polar cusp position by low altitude satellites have shown that the boundary of the cusp moves equatorward for the southward turning of the IMF B_z-component (Burch, 1973; Friis-Christensen, 1986; Meng, 1983; Newell and Meng, 1987; Newell et al., 1989; Russell et al., 1971). *Newell and Meng* [1987] stated that the cusp narrows for the IMF B_z <0 and attribute this to enhanced tailward convection of magnetic flux.

Observations of the dayside auroral oval from ground observations (Feldsten and Starkov, 1967; Horwitz and Akasofu, 1977; Sandholt et al., 1986; Sandholt et al., 1989) showed that the dayside auroral oval shifts equatorward(poleward) when the IMF B_z-component is negative(positive). During the periods when the dayside auroral oval is expanding, poleward-moving auroral forms (PMAFs) are observed moving away from the dayside auroral oval into the polar cap (Drury et al., 2003; Fasel et al., 1994b; Fasel et al., 1992; Horwitz and Akasofu, 1977; Sandholt et al., 1986; Vorobjev et al., 1975; Xing et al., 2012) Both Vorobjev et al. (1975) and (Horwitz and Akasofu, 1977) attributed these PMAFs to magnetic flux being eroded from the dayside magnetopause and transported antisunward.

Combined ground-based optical and low altitude satellites observations have shown optical auroral events moving from the region with cusp/low-latitude boundary particle precipitation into that of mantle precipitation (Denig et al., 1993; Sandholt et al., 1993). Elphic et al. (1990) reported the first direct link of FTEs to PMAFs by using simultaneous ISEE spacecraft, radar, and ground optical data.

A few studies have connected the antisunward motion of the PMAFs with plasma flow via radar data, as they move from the dayside auroral oval into the polar cap [Oksavik et al., 2005; P E Sandholt et al., 1990]. Pudovkin et al. (1996) related the speed of the PMAF to the magnetopause electric field intensity. *Kan and Lee* [1979] found an expression for the polar cap electric field (E_{pc}), sometimes called the Kan-Lee electric field (E_{KL}), $E_{KL} = E_{pc} = v_{sw}B_{sw}\sin^2\frac{\phi}{2}$, where ϕ is the projection of the polar angle of the IMF onto the *yz*-plane in the solar-magnetosphere coordinates, v_{sw} is the solar wind speed and B_{sw} is the total magnitude of the IMF (Kan and Lee, 1979). Hence, the ionospheric PMAF speed, $v_{PMAF} = \frac{E_{pc}}{B_{pc}}$, may depend on both v_{sw} and the IMF components B_y and B_z. The present paper examines the dependence of PMAF motion into the polar cap with respect to the solar wind speed, using both v_{flow} (flow speed) and v_x (x-component of the solar wind speed). PMAFs are identified by using both the colored all-sky camera (ASC) and meridian scanning photometer (MSP), which plots the elevation angle (the angle which the MSP sweeps out from the southern horizon through the zenith to the northern horizon, the magnetic meridian) versus time. The signature of the PMAF on the MSP is slanted, see Figures 1, 3 (Fasel et al., 1995). In Figure 3, a black is line drawn through the PMAF's a and b.

Figure 2 represents an MSP plot, with the black line representing a PMAF signature. α_{PMAF} is angle the PMAF makes with the horizontal (Time) axis of the MSP emission plots. NOTE: this angle is dependent upon the choice of aspect ratio and the axis ranges of the emission plots. The PMAF-SLOPE, v_α [$v_\alpha = \frac{\Delta(EA)}{\Delta T}$], is the slope of the slanted line; where EA is the elevation angle and T is the time. The PMAF-SLOPE v_α has units of elevation angle/time. PMAF signatures on the MSP emission plots, see Figures 1, 3, are similar to the linear relationship obtained from a distance versus time plot for a moving object. Larger PMAF-SLOPES or angles

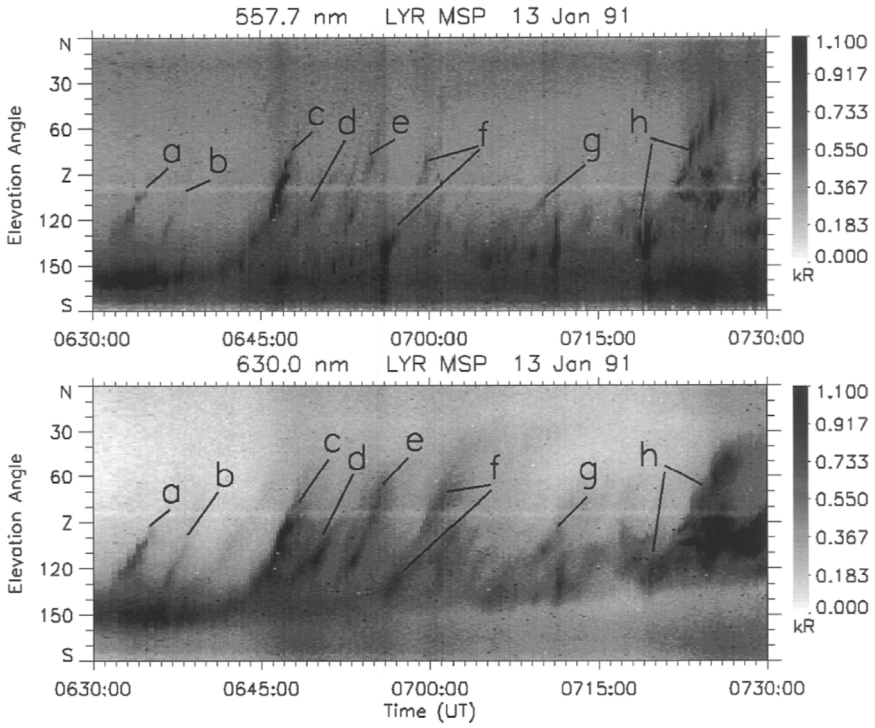

FIGURE 1
MSP grayscale plot showing the intensity of the [OI] 557.7 nm (top panel) and [OI] 630.0 nm (bottom panel) emissions for 13 January 1991 from Longyearbyen, Norway. The auroral line emission intensities are plotted as a function of the elevation angle along the magnetic meridian. Poleward-moving auroral forms (PMAFs) are indicated by lower case letters. Note that each PMAF (a, b, c, d, e, f, g, and h) have approximately the same slant signature, making an angle α_{PMAF} (which will be measured in this study) with the horizontal axis (Time axis) of the MSP emission plots, for the specific aspect ratio and axes ranges of the above plots.

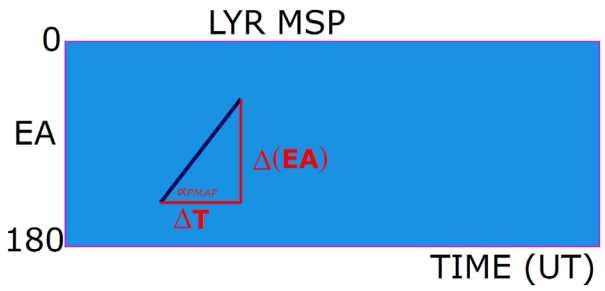

FIGURE 2
A Meridian Scanning Photometer (MSP) plot is represented by the above cartoon. The elevation angle (EA), where the MSP sweeps through 0–180° every 8 s, is the vertical axis. Time (in UT) is the horizontal axis. The black slanted line represents a PMAF. α_{PMAF} is the angle the black slanted line (PMAF) makes with the time axis for the specific plot panels used here. The PMAF-SLOPE is defined by $v_\alpha = \frac{\Delta(EA)}{\Delta T}$.

(α_{PMAF}) indicate higher speeds. The hypothesis is, higher PMAF-SLOPEs, v_α (or larger α_{PMAF}), are associated with higher solar wind speeds. Therefore, PMAF motion is consistent with expectations from dayside reconnection and are related to both the IMF and the GMF.

2 Ground-based optical and satellite data

The Meridian Scanning Photometer (MSP) and BACC colored All-Sky Camera (ASC) are located at the Kjell Henriksen Observatory, located in Longyearbyen, Svalbard (GEO: 78.148° N, 16.043° E; AACGM: 75.24° N, 111.21° E).

The PMAF emissions from the [OI] 630.0 nm red line and the [OI] 557.7 nm green line are analyzed using the meridian scanning photometer (MSP) (Fasel et al., 1994a). Auroral line emission intensities are plotted as function of the elevation angle along the magnetic meridian. The MSP has a spatial resolution of 1° and makes a scan along the magnetic meridian, from the southern to the northern horizon, every 8 s. A plot is constructed using the elevation angle and the time in UT. Figures 1, 3 are MSP emission plots, each containing several PMAFs. Each figure contains both the [OI] 557.7 nm green line emission and the [OI] 630.0 nm red line emission. The PMAF events, in both the ASC and MSP, are identified by lower case letters; see Figures 1, 3. Every PMAF event originates at the dayside auroral oval which was south of the zenith and then moves anti-sunward into the polar cap. The drawn slanted lines on the MSP in Figure 3 indicate motion, similar to a distance versus time graph. The PMAF-SLOPE, v_α, is the slope of the drawn slanted line with units of (elevation angle)/time.

The ASC instrument is designed to capture the visible part of the electromagnetic spectrum, 4,000–7,000 Å and captures the

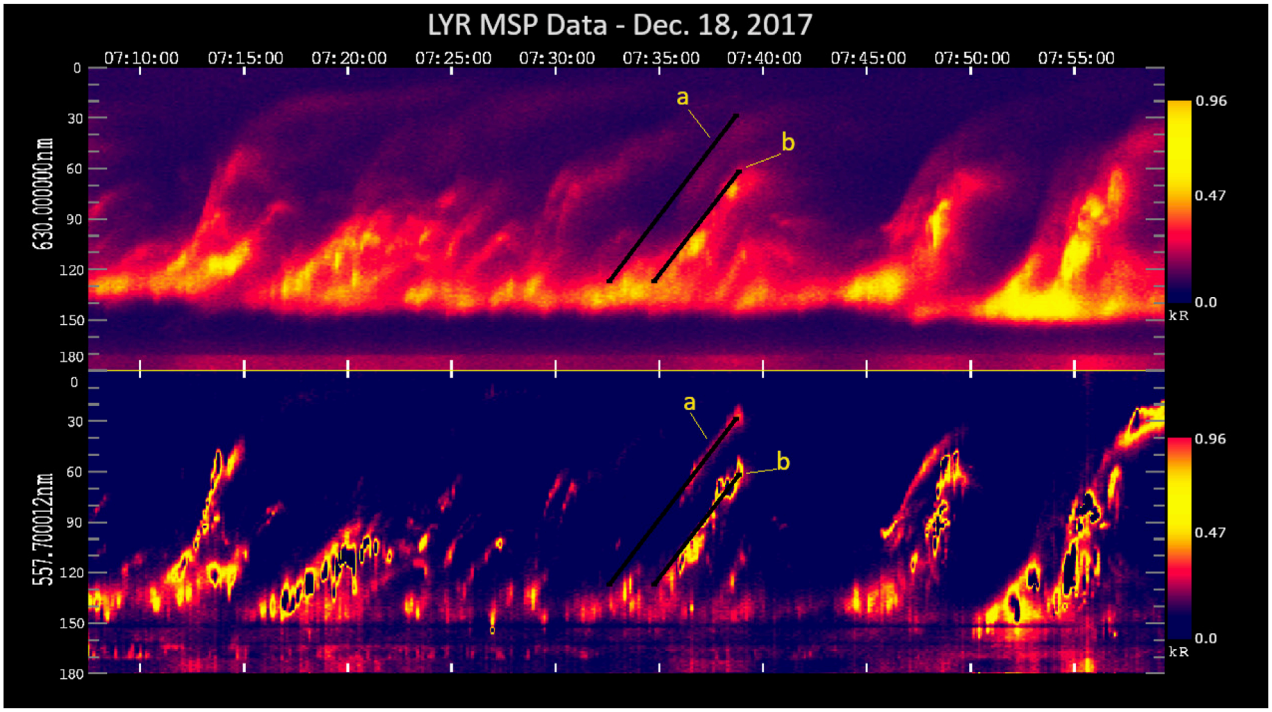

FIGURE 3
MSP plot showing the intensity of the [OI] 630.0 nm (top panel) and [OI] 557.7 nm (bottom panel) emissions for 18 December 2017 from the Kjell Henriksen Observatory; Longyearbyen, Norway. The axes are the same as Figure 1. PMAFs are labeled a and b. The black lines are drawn between the start and end times of each PMAF event. These times are obtained using both the MSP and ASC data. The PMAF-SLOPE, $v_{\alpha'}$ is the slope of the black slanted line. α_{PMAF} is the angle the slated line makes with the horizontal (Time axis) of the MSP emission plot, for the specific plot panels used in this figure.

evolution of each PMAF as it moves into the polar cap (Fasel and Sigernes, 2022). The PMAF never loses its identity during its lifetime, i.e., the poleward moving auroral arc or rayed band never disappeared from the optical instruments and then appeared again further north of its previous position. Observations are restricted to the dayside between 0630 and 1030 UT, so that the data collected are due to the direct interaction between the solar wind and the magnetopause. Figure 4 (A–I) shows the evolution of PMAF events a and b. Figure 4A shows the start of PMAF event a at 07:32:00 UT. By 07:32:25 UT PMAF event a is moving poleward. In Figure 4B, the auroral oval begins to brighten on the poleward edge in the east (E). Figure 4C at 07:35:30 UT, shows PMAF event a crossing the zenith (W-E line) with PMAF event b just leaving the expanded dayside auroral oval. Also notice in Figure 4C how the brightening in PMAF event b has westward when compared to Figure 4B. Figures 4D–F shows both PMAF events a and b propagating anti-sunward, towards the northwest (NW, geographical). PMAF events a and b can be observed fading in brightness as they propagate anti-sunward in frames 4G-I. PMAF event b does not drift as far as PMAF event b. This can also be observed in the MSP emission plots in Figure 3. Both PMAF events (a and b) are labeled on the MSP plot in Figure 3.

Satellite shifted to bow shock-nose (BSN) data from WIND, ACE, and DSCOVR are used to determine the solar wind speed for each PMAF event. The x-component v_x, of the solar wind speed and v_{flow} (flow speed) are used for this study. Figure 5 contains the IMF conditions for 18 December 2017. The IMF is southward which is conducive for dayside reconnection.

Figure 5 is the calculated clock angle between 06:00 UT and 08:20 UT. The IMF clock angle (θ_{IMF}) is obtained by projecting the IMF vector onto the Geocentric Solar Magnetic (GSM) yz-plane and finding: $\theta_{IMF} = \tan^{-1}\left(\frac{B_y}{B_z}\right)$. θ_{IMF} is the angle between the projected IMF vector and GSM north z ($+z$). The clock angle is dependent on the speed of the solar wind, as higher speeds are associated with larger θ_{IMF} and *vice versa* (Zhang et al., 2019).

Figure 5 contains 21 PMAFs generated (18 December 2017) during the clock angle interval in Figure 6. Two (PMAF events a and b) of the fifty-seven PMAF events are shown in Figures 3, 4 (MSP, ASC). The 57 events (day and start time for each event) used in this study are found in Table 1.

The x-component of the solar wind speed, v_x, is ~594 km/s for PMAF events a and b, with the clock angle for both PMAFs greater than 100. The angle (α_{PMAF}) PMAF event "a" makes with the horizontal of the MSP emission plot is $\alpha_{PMAF} = 55.923°$ and $\alpha_{PMAF} = 56.1°$ for PMAF event "b".

3 Analysis

All of the PMAF events for this study were identified using both the meridian scanning photometer (MSP) and the colored ASC. Note that the PMAFs for each day have a similar slanted signature,

10.3389/fspas.2023.1233060

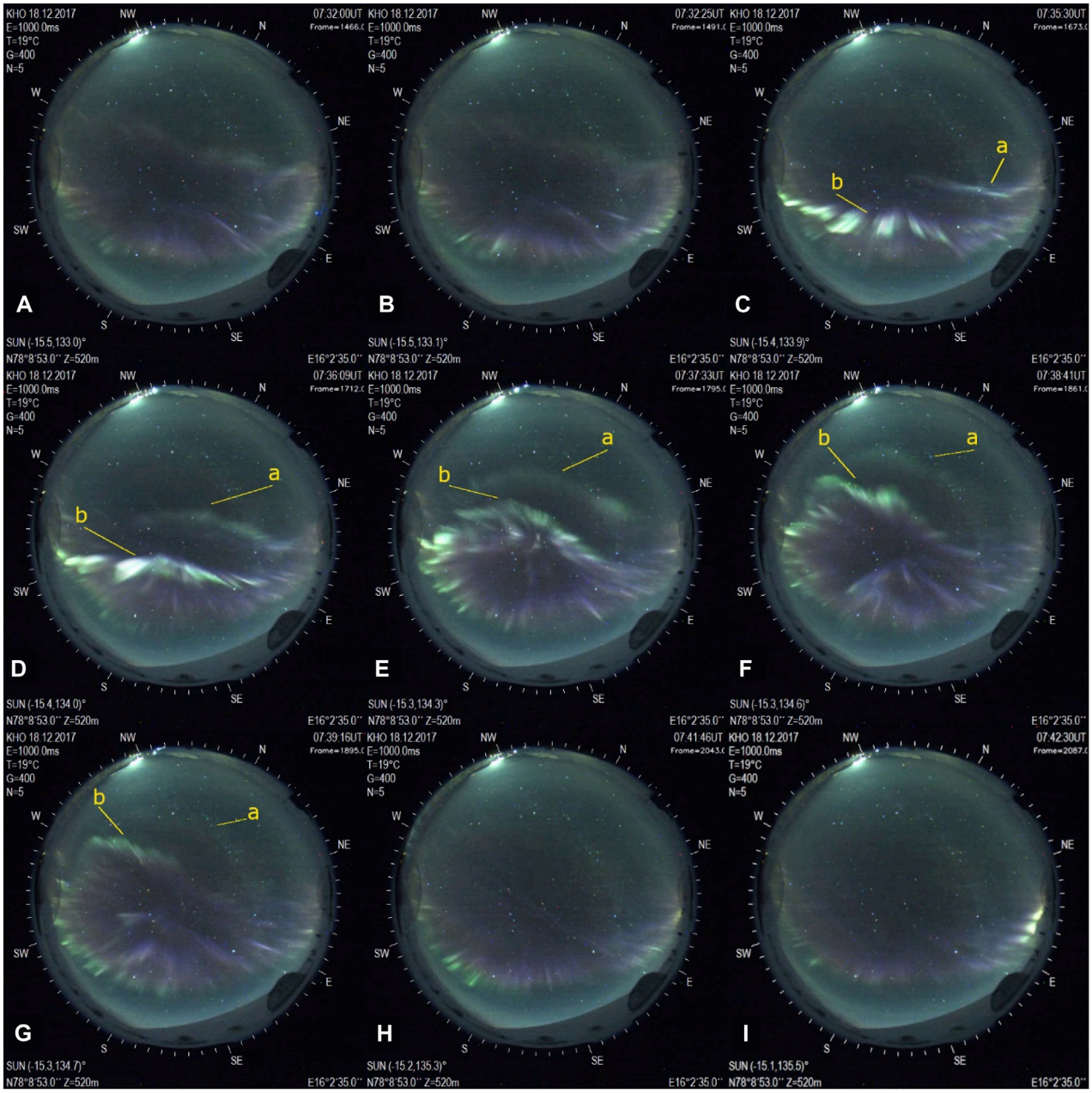

FIGURE 4
All-sky camera images are from the Kjell Henriksen Observatory in Longyearbyen, Norway for 18 December 2017. PMAF events are indicated by a and b, which are yellow in color. Each frame is labeled with capital letter, **(A-I)**. these labels represent the time evolution of the PMAF events a and b. 4B shows the begininning of pmaf event A, at the poleward edge of the dayside auroral oval. **(G-I)** show PMAF events a and b fading from view at the end of their anti-sunward journey. These are the same PMAF events indicated in the MSP plot in Figure 5.

see Figure 1 for multiple examples of PMAFs during a 1-h interval. This indicates that PMAF events for each interval move at roughly the same rate through the polar cap away from the dayside auroral oval. This study will compare the PMAF-SLOPE and α_{PMAF}, the angle the slanted PMAF signatures make with respect to with the horizontal (time axis) on the MSP plot panels (see Figures 1–3), with the v_x (x-component of the solar wind speed) and v_{flow} (flow speed).

This study contains 57 PMAFs. The PMAFs' start and stop times were determined using both the [OI] 557.7 nm green line emission, the [OI] 630.0 nm red line emissions and the colored all-sky camera. A density plot from the colored ASC (Fasel and Sigernes, 2022) was made for each PMAF event. First, the ASC data were used to identify the PMAFs. To identify the PMAF on the MSP, both the ASC and density plot for each PMAF event are used to determine when the PMAF begins to separate from the dayside auroral oval and move anti-sunward. The MSP intensities were varied until a clear starting point on each emission plot was determined and could be correlated with the beginning of the poleward motion of the PMAF

10.3389/fspas.2023.1233060

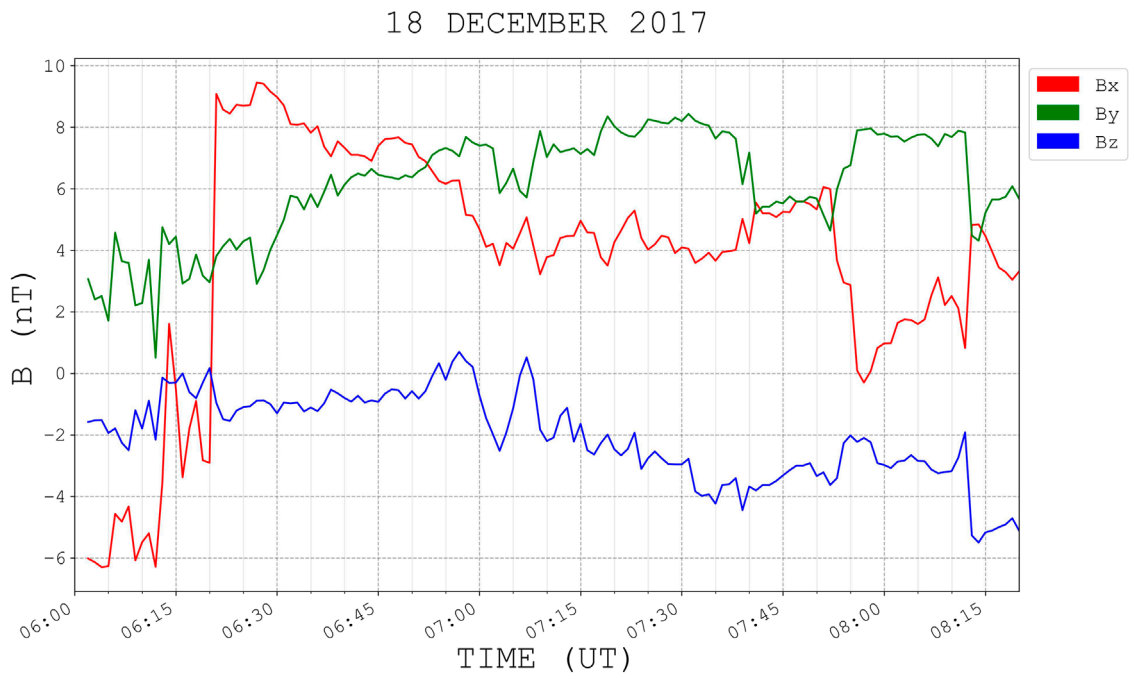

FIGURE 5
IMF data [1 min bow shock-nose (BSN)-time shifted data] from DSCOVR spacecraft ($X_{GSE} \approx 231.36\ R_E$, $Y_{GSE} \approx 39.58\ R_E$, $Z_{GSE} \approx -4.7\ R_E$) for 18 December 2017: IMF components.

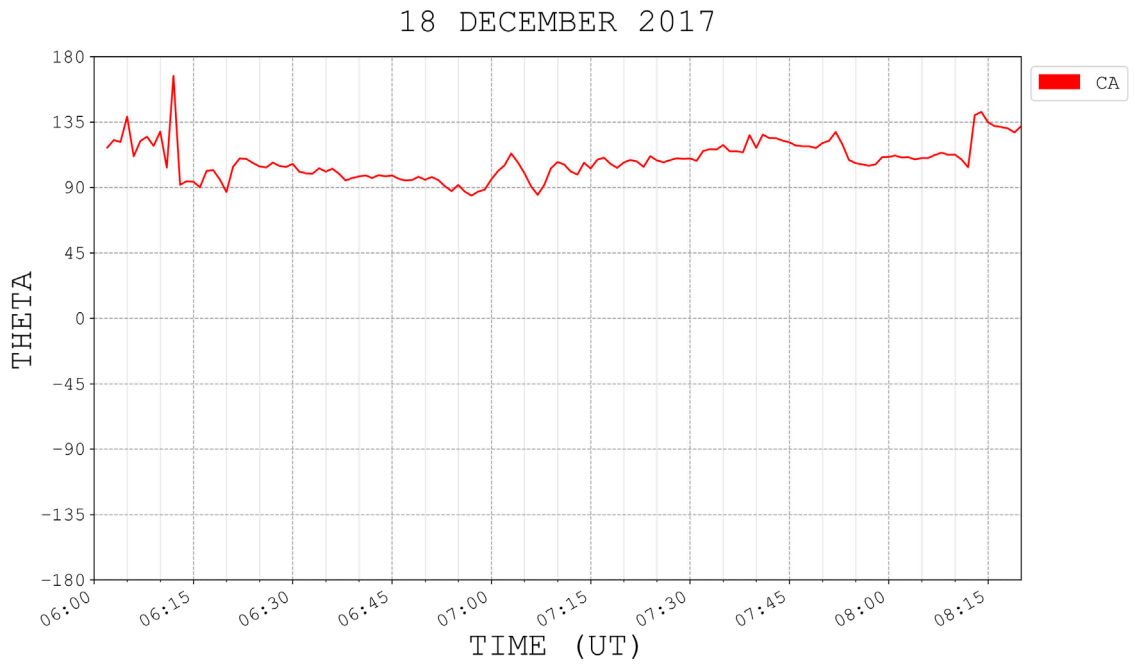

FIGURE 6
The clock angle (CA in red) obtained from the IMF data in Figure 5. 21 PMAFs in Figure 6 occurred during this interval, which was favorable for dayside magnetic reconnection and $v_x \geq 594.5 \frac{km}{s}$.

on the ASC and density plots. Initially, the [OI] 557.7 nm green line emission is used to identify the start and stop times of the PMAF events. The [OI] 630.0 nm red line emission is also viewed to see if a similar start and stop time matched the green line emission. Several points were selected for each PMAF event to determine its slanted line signature on the MSP. After the PMAF slanted line is

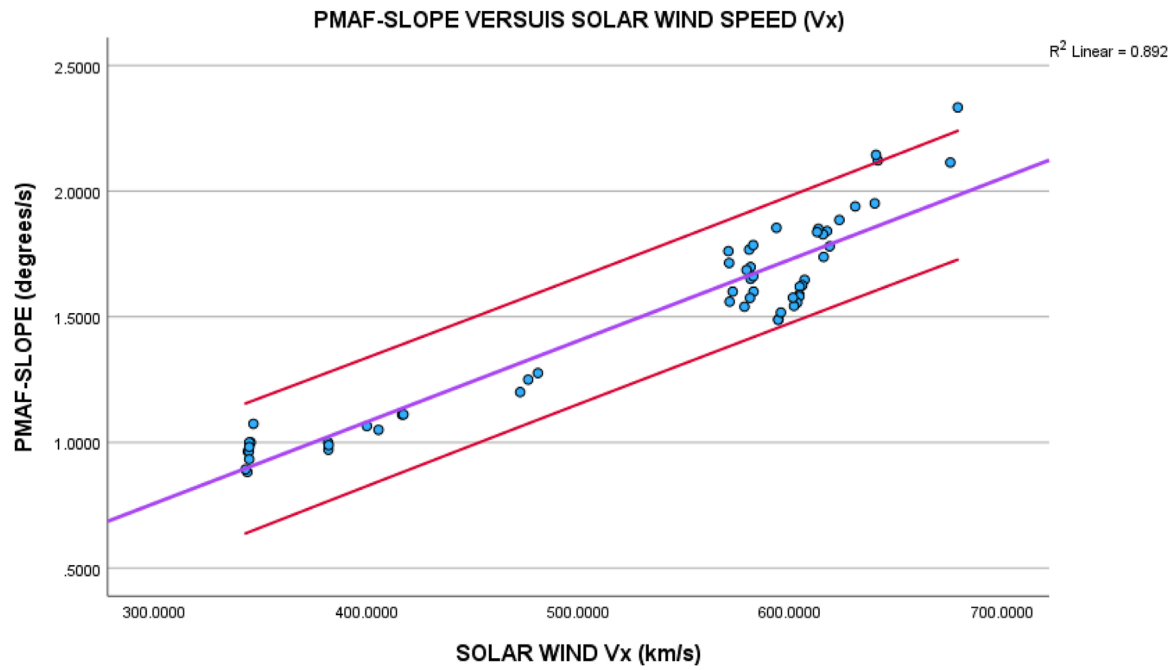

FIGURE 7
The horizontal axis of this plot contains the average solar wind speed (v_x-component), which is averaged around the start time of the PMAF event; 3 min before and 3 min after the start time of the PMAF event. The vertical axis of this plot consists of the PMAF-SLOPE, $v_\alpha = \frac{\Delta(EA)}{\Delta T}$. The linear regression coefficient is $r_{v_\alpha} = 0.944$.

identified on the MSP, two points are selected (start and stop) to find v_α and α_{PMAF}. Each point (start and stop) has 2 coordinates, elevation angle and time, which are extracted from the MSP data. The time (in UT) and elevation angle, 0–180°, is recorded by the MSP as it sweeps through the magnetic meridian every 8 s. These points are used to calculate Δ(EA), Δ**T**, and α_{PMAF}, for each PMAF event, See Table 1. After clicking first, the start and then the stop point, the MSP program calculates α_{PMAF} using arctan (slope) and draws a line from the starting point to the stopping point on the MSP emission figures. The angle, $\alpha_{PMAF,}$ is between the drawn slanted line and the horizontal (time axis) on the MSP emission plot, for this choice of aspect ratio and ranges of the axes. Figure 3 shows PMAF events a and b with lines drawn through the PMAF. This procedure was followed for each PMAF event.

After v_α and α_{PMAF} are determined for all the PMAFs, these values were plotted against the solar wind speed (v_x-component) and flow speed. Figure 7 shows the PMAF-SLOPE versus the solar wind speed(v_x-component). This figure shows the linear relationship between PMAF-SLOPE and v_x. The linear regression coefficient (r) calculated for the linear regression plot is $r_{v_\alpha} = \mathbf{0.944}$ (Pearson Correlation Coefficient) (Ross, 2014).

Figure 8 plots α_{PMAF} against the solar wind flow speed v_x-component. This figure shows a very strong linear relationship between α_{PMAF} and v_x, $r_{\alpha PMAF} = \mathbf{0.973}$. Figure 9 is similar to Figure 8, with the solar wind flow speed, v_{flow}, replacing v_x. There is a very strong linear regression coefficient, r = 0.9726, between α_{PMAF} and v_{flow}. The difference between "slope" and "alpha" is an arctan function, which should provide constraints on the physical mechanism leading the relationship between the PMAF motion and the solar wind parameters (since "alpha" is a derived metric, has a stronger correlation than "slope", the physical observation.)

4 Discussion and conclusion

Magnetic reconnection at the subsolar magnetopause occurs when the IMF B_z component turns southward, $B_z>0$ to $B_z<0$. This process provides a number of observable events as shown by numerous satellite and ground observations:

(1) Earthward displacements of the dayside magnetopause (Aubry et al., 1970; Meng, 1970),
(2) Equatorward displacements of the cusp (Burch, 1973; Meng, 1983; Newell et al., 1989; Russell et al., 1971),
(3) Equatorward displacement of the dayside auroral oval (Feldsten and Starkov, 1967; Horwitz and Akasofu, 1977; Sandholt et al., 1986),

One would expect to observe ionospheric signatures generated from magnetic reconnection at the subsolar magnetopause which causes the above three displacements (Drury et al., 2003; Fasel, 1995; Horwitz and Akasofu, 1977; Sandholt et al., 1990; Vorobjev et al., 1975; Xing et al., 2012). PMAFs are considered as possible candidates for ionospheric signatures of magnetic flux erosion from the dayside magnetopause (Fasel, 1995; Fasel et al., 1993; Lockwood, 1991; Sandholt et al., 1986; Vorobjev et al., 1975).

If PMAFs are the result of magnetic reconnection, their movement into the polar cap should be dependent on the solar wind speed. Figures 7–9 provide very good linear relationships between PMAFs and the solar wind speed (either v_x or v_{flow}). All the points

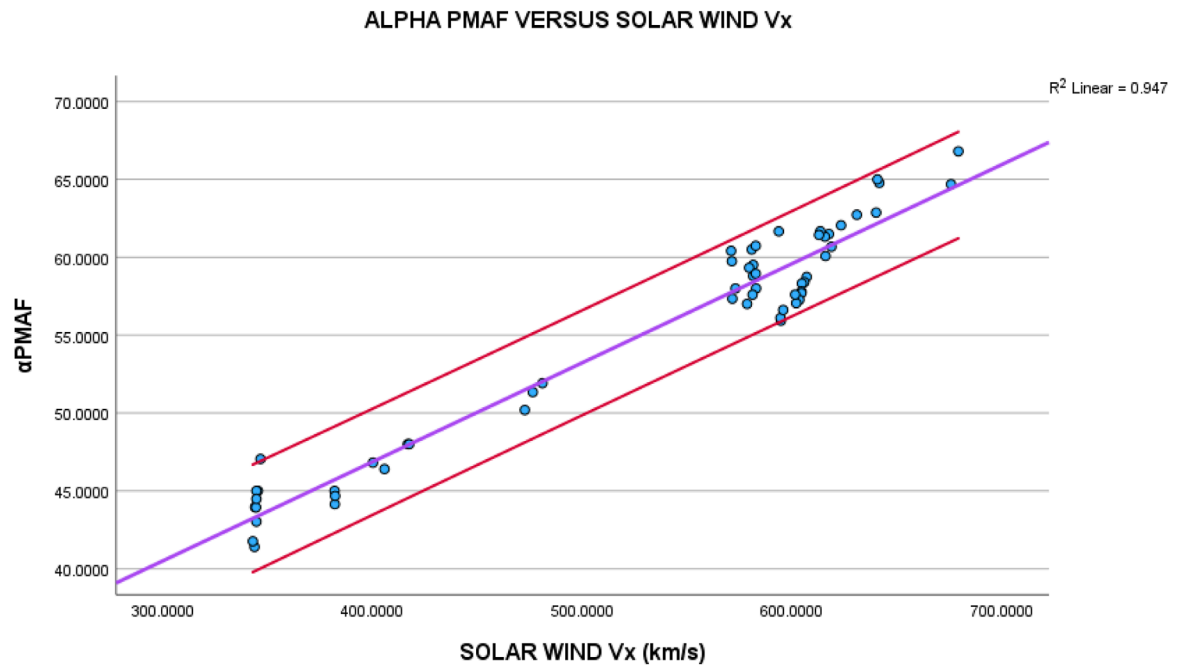

FIGURE 8
The horizontal axis of this plot contains the average solar wind speed (v_x-component), which is averaged around the start time of the PMAF event; 3 min before and 3 min after the start time of the PMAF event. The vertical axis of this plot consists of the angle (α_{PMAF}) the PMAF makes with the horizontal axis of the MSP (its time axis). The linear regression coefficient is $r_{\alpha PMAF} = 0.973$.

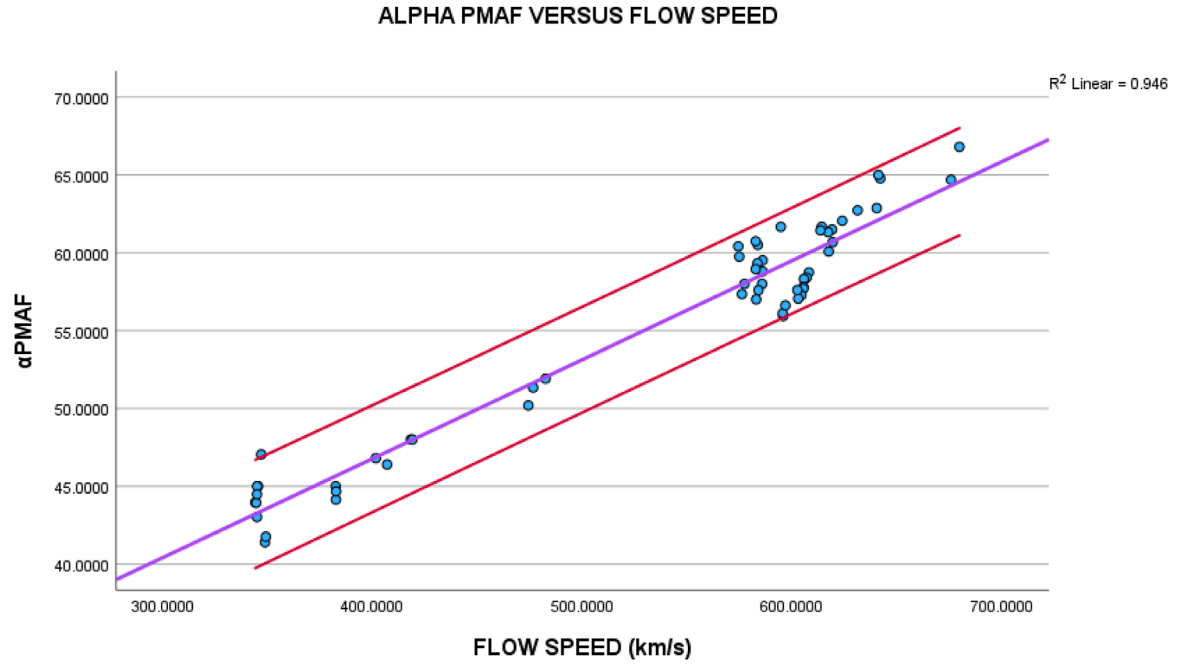

FIGURE 9
The horizontal axis of this plot contains the average solar wind flow speed v_{flow}, which is averaged around the start time of the PMAF event; 3 min before and 3 min after the start time of the PMAF event. The vertical axis of this plot consists of the angle (α_{PMAF}) the PMAF makes with the horizontal axis of the MSP (its Time axis). The linear regression coefficient is r = 0.9726.

10.3389/fspas.2023.1233060

TABLE 1 The 57 PMAF events used in this study, which includes the date, start time, α_{PMAF}, v_{flow} (flow speed), and v_x (x-component of the solar wind speed).

DATE	Start time	α_{PMAF}	v_α	SW speed	
18-Dec-01		degrees	$\frac{\text{degrees}}{\text{s}}$	FLOW (km/s)	V_x (km/s)
1	6:23:17 UT	51.34	1.25	476.5	476.3
2	6:36:13 UT	50.194	1.2	474.2	472.5
3	6:38:37 UT	51.911	1.276	482.4	480.9
10-Dec-07					
1	6:10:30 UT	43.958	0.964	344.09	343.957
2	6:13:10 UT	43.939	0.964	344.5	344.4
3	6:16:22 UT	45	1	345.42	345.32
4	6:25:26 UT	45	1	344.94	344.61
5	6:39:50 UT	43.025	0.933	344.9	344.59
6	6:41:10 UT	44.484	0.982	344.91	344.59
7	7:09:10 UT	47.045	1.074	346.93	346.56
29-Dec-11					
1	6:41:05 UT	41.4	0.882	348.7	343.7
2	6:44:17 UT	41.76	0.893	349.1	342.9
17-Dec-12					
1	7:57:00 UT	46.81	1.065	401.54	400.14
2	8:00:44 UT	46.4	1.05	406.9	405.64
3	8:20:27 UT	48.0	1.11	418.19	416.73
4	8:23:07 UT	48.0	1.111	418.9	417.41
27-Nov-16					
1	6:06:12 UT	61.489	1.841	618.91	617.39
2	6:07:08 UT	60.078	1.738	617.33	615.78
3	6:51:00 UT	58.799	1.651	585.814	581.3
4	6:51:16 UT	59.507	1.698	585.81	581.3
5	6:54:28 UT	57.002	1.54	582.77	578.4
6	6:58:59 UT	59.323	1.686	583.39	579.39
7	7:05:39 UT	57.995	1.6	577.19	572.86
8	7:08:11 UT	57.339	1.56	575.99	571.4
9	7:18:43 UT	60.499	1.767	583.53	580.62
10	7:20:11 UT	60.736	1.785	582.53	582.53
11	7:20:19 UT	58.946	1.661	582.53	582.53

(Continued on the following page)

TABLE 1 (*Continued*) **The 57 PMAF events used in this study, which includes the date, start time, α_{PMAF}, v_{flow} (flow speed), and v_x (x-component of the solar wind speed).**

DATE	Start time	α_{PMAF}	v_α	SW speed	
18-Dec-01		degrees	$\frac{\text{degrees}}{\text{s}}$	FLOW (km/s)	V_x (km/s)
12	7:21:15 UT	57.995	1.6	585.59	582.69
13	7:25:07 UT	57.593	1.575	583.84	581.03
14	8:02:11 UT	59.744	1.714	574.7	571.16
15	8:03:23 UT	60.408	1.761	574.23	570.81
10-Dec-16					
1	8:52:05 UT	66.801	2.333	679.6	679.1
2	8:52:46 UT	64.687	2.114	675.6	675.6
18-Dec-17					
1	6:16:10 UT	61.661	1.854	594.5	593.5
2	6:30:18 UT	62.865	1.951	640.2	639.9
3	6:33:30 UT	64.772	2.122	641.9	641.4
4	6:35:06 UT	64.993	2.144	641	640.5
5	6:39:29 UT	62.723	1.939	631.1	630.7
6	6:49:37 UT	62.049	1.885	623.8	623.2
7	6:53:57 UT	60.673	1.78	619.2	618.6
8	6:57:05 UT	61.32	1.828	617.1	615.5
9	6:58:57 UT	61.67	1.85	614	613.3
10	7:02:37 UT	61.434	1.837	613.4	612.7
11	7:11:05 UT	58.736	1.647	607.9	606.8
12	7:13:45 UT	58.4	1.625	606.8	605.7
13	7:17:21 UT	58.314	1.62	605.5	604.5
14	7:19:05 UT	57.804	1.588	605.3	604.3
15	7:22:57 UT	57.693	1.581	605.3	604.3
16	7:24:25 UT	57.265	1.556	604.3	603.3
17	7:25:13 UT	57.051	1.543	602.8	601.8
18	7:35:45 UT	55.923	1.49	595.6	594.5
19	7:34:57 UT	56.1	1.488	595.4	594.3
20	7:37:05 UT	56.612	1.517	596.7	595.6
21	7:45:21 UT	57.6	1.576	602.4	601.3

(Continued on the following page)

TABLE 1 (*Continued*) **The 57 PMAF events used in this study, which includes the date, start time, α_{PMAF}, v_{flow} (flow speed), and v_x (x-component of the solar wind speed).**

DATE	Start time	α_{PMAF}	v_α	SW speed	
18-Dec-01		degrees	$\frac{\text{degrees}}{\text{s}}$	FLOW (km/s)	V_x (km/s)
20-Nov-20					
1	6:26:05 UT	44.145	0.971	382.52	381.97
2	6:27:57 UT	45	1	382.414	381.843
3	6:33:17 UT	44.673	0.9889	382.6	382.1

(blue) fall within the 95% confidence interval indicated by the two red parallel slanted lines, nestled close to the purple fit line. The probability p is 0.001 that the correlation coefficient will be greater than 0.872 (Fisher and Yates, 1963), which implies that the correlation coefficients obtained in this study were not obtained by chance. This indicates a strong linear relationship between the solar wind speed and the PMAFs' movement away from the dayside auroral oval, anti-sunward, into the polar cap. The linear regression coefficients from this study are: $r_{v_\alpha} = \mathbf{0.944}$ and $r_{\boldsymbol{\alpha} PMAF} = \mathbf{0.973}$.

The following statement can be made regarding this analysis: the anti-sunward movement of the PMAFs into the polar cap depends on the solar wind speed (either the flow speed or the v_x-component); the PMAF-SLOPE v_α (or α_{PMAF}) increases as the solar wind speed increases (flow speed, v_{flow}, or the v_x-component). However, the v_x-component is a better fit, perhaps providing constraints as to the actual mechanism relating the degrees per time motion, and the solar wind parameters.

The strong correlation obtained from this study strongly suggests that PMAFs are indeed the ionospheric footprints of a newly formed magnetic flux tube due to dayside magnetic reconnection. The following conclusions are obtained from this statistical study:

(i) the PMAF-SLOPE v_α is highly correlated ($r_{v_\alpha} = \mathbf{0.944}$) to the v_x-component of the solar wind, increasing when v_x increases and *vice versa*,

(ii) α_{PMAF} is highly correlated ($r_{\boldsymbol{\alpha} PMAF} = \mathbf{0.973}$) to the v_x-component of the solar wind, increasing when v_x increases and *vice versa*,

(iii) PMAFs must be connected to both the IMF and GMF and are dragged anti-sunward, mostly by the v_x-component of the solar wind,

(iv) PMAF's are indeed the ionospheric footprints of a newly formed magnetic flux tube, due to dayside magnetic reconnection, being transferred from the dayside to nightside (Horwitz and Akasofu, 1977; Vorobjev et al., 1975).

Data availability statement

The datasets presented in this study can be found in online repositories. The names of the repository/repositories and accession number(s) can be found in the article/Supplementary Material.

Author contributions

GF: Designed the study analyzed data, and wrote the manuscript. LL: Collaborated and provided edits to the manuscript. EL: Analyzed data. DC: Analyzed data. BY: Wrote software to analyze data. OB: Formal analysis, Writing–original draft. JB: Data curation, Formal analysis, Writing–original draft and Analyzed data. SL: Provided satellite data. JM: Wrote software to analyze all-sky camera data. FS: Provided the all-sky camera data. DL: Provided meridian scanning photometer data. All authors contributed to the article and approved the submitted version.

Funding

KECK Grant: Funded student researcher's during the Academic year and summer research.

Acknowledgments

The authors would like to thank FS and DL for use of the All-sky camera data archived at the Kjell Henriksen Observatory. More information on the Boreal Aurora Camera Constellation is also available via this link: http://kho.unis.no/. GF would like to thank Stephen Mende and Yen-Jung Wu (Space Sciences Laboratory, University of California, Berkeley) for their helpful discussions. The authors would like to thank FS, Chief Scientist at the Kjell Henriksen Observatory, for the ground-based optical data (all-sky camera and meridian scanning photometer). The authors would also like to thank NASA for providing access to their satellite data.

Conflict of interest

The authors declare that the research was conducted in the absence of any commercial or financial relationships that could be construed as a potential conflict of interest.

Publisher's note

All claims expressed in this article are solely those of the authors and do not necessarily represent those of their affiliated

organizations, or those of the publisher, the editors and the reviewers. Any product that may be evaluated in this article, or claim that may be made by its manufacturer, is not guaranteed or endorsed by the publisher.

References

Aubry, M. P., Russell, C. T., and Kivelson, M. G. (1970). Inward motion of the magnetopause before a substorm. *J. Geophys. Res.* 75 (34), 7018–7031. doi:10.1029/JA075i034p07018

Berchem, J., and Russell, C. T. (1984). Flux transfer events on the magnetopause: spatial distribution and controlling factors. *J. Geophys. Res. Space Phys.* 89 (A8), 6689–6703. doi:10.1029/JA089iA08p06689

Burch, J. L. (1973). Rate of erosion of dayside magnetic flux based on a quantitative study of the dependence of polar cusp latitude on the interplanetary magnetic field. *Radio Sci.* 8 (11), 955–961. doi:10.1029/RS008i011p00955

Daly, P. W., Saunders, M. A., Rijnbeek, R. P., Sckopke, N., and Russell, C. T. (1984). The distribution of reconnection geometry in flux transfer events using energetic ion, plasma and magnetic data. *J. Geophys. Res. Space Phys.* 89 (A6), 3843–3854. doi:10.1029/JA089iA06p03843

Denig, W. F., Burke, W. J., Maynard, N. C., Rich, F. J., Jacobsen, B., Sandholt, P. E., et al. (1993). Ionospheric signatures of dayside magnetopause transients: a case study using satellite and ground measurements. *J. Geophys. Res. Space Phys.* 98 (A4), 5969–5980. doi:10.1029/92JA01541

Drury, E. E., Mende, S. B., Frey, H. U., and Doolittle, J. H. (2003). Southern Hemisphere poleward moving auroral forms. *J. Geophys. Res. Space Phys.* 108 (A3). doi:10.1029/2001ja007536

Dungey, J. W. (1961). Interplanetary magnetic field and the auroral zones. *Phys. Rev. Lett.* 6 (2), 47–48. doi:10.1103/PhysRevLett.6.47

Elphic, R. C., Lockwood, M., Cowley, S. W. H., and Sandholt, P. E. (1990). Flux transfer events at the magnetopause and in the ionosphere. *Geophys. Res. Lett.* 17 (12), 2241–2244. doi:10.1029/GL017i012p02241

Fasel, G. J. (1995). Dayside poleward moving auroral forms: a statistical study. *J. Geophys. Res. Space Phys.* 100 (A7), 11891–11905. doi:10.1029/95ja00854

Fasel, G. J., Lee, L. C., and Smith, R. (Editors) (1995). *Dayside poleward moving aurroal forms: a brief review* (Washingto, D.C: American Geophysical Union), 439–447. doi:10.1029/GM090p0439

Fasel, G. J., Lee, L. C., and Smith, R. W. (1993). A mechanism for the multiple brightenings of dayside poleward-moving auroral forms. *Geophys. Res. Lett.* 20 (20), 2247–2250. doi:10.1029/93GL02487

Fasel, G. J., Minow, J. I., Smith, R. W., Deehr, C. S., and Lee, L. C. (1992). Multiple brightenings of transient dayside auroral forms during oval expansions. *Geophys. Res. Lett.* 19 (24), 2429–2432. doi:10.1029/92GL02103

Fasel, J. M., and Sigernes, F. (2022). "Chapter 5 - magnetospheric imaging via ground-based optical instruments," in *Understanding the Space environment through global measurements*. Editors Y. Colado-Vega, D. Gallagher, H. Frey, and S. Wing (China: Elsevier), 217–229. doi:10.1016/B978-0-12-820630-0.00001-5

Fasel, L., Minow, J. I., Lee, L. C., Smith, R. W., and Deehr, C. S. (1994a), Poleward-moving auroral forms: what do we really know about them? in *Physical signatures of magnetospheric boundary layer processes. NATO ASI series (series C: mathematical and physical Sciences)*, edited by E. A. Holtet, pp. 211–226. Springer, Dordrecht. doi:10.1007/978-94-011-1052-5_15

Fasel, L., Minow, J. I., Smith, R. W., Deehr, C. S., and Lee, L. C. (1994b). "Multiple brightenings of poleward-moving dayside auroral forms," in *Solar wind sources of magnetospheric ultra-low-frequency waves*. Editors K. T. M. Engebretson, and M. Scholer (USA: ANGEO), 201–211. doi:10.1029/GM081p0201

Feldsten, Y. I., and Starkov, G. V. (1967), *Dynamics of auroral belt polar geomagnetic disturbances*, 209–229. doi:10.1016/0032-0633(67)90190-0

Fisher, R. A., and Yates, F. (1963). *Statistical tables for biological, agricultural and medical research*. 6th ed. Edinburgh: Oliver & Boyd.

Friis-Christensen, E. (1986), Solar wind control of the polar cusp, in *Sol. Wind Magnetos. Coupling*, edited, p. 423. doi:10.1007/978-90-277-2303-1_31

Haerendel, G., Paschmann, G., Sckopke, N., Rosenbauer, H., and Hedgecock, P. C. (1978). The frontside boundary layer of the magnetosphere and the problem of reconnection. *J. Geophys. Res. Space Phys.* 83 (A7), 3195–3216. doi:10.1029/JA083iA07p03195

Horwitz, J. L., and Akasofu, S.-I. (1977). The response of the dayside aurora to sharp northward and southward transitions of the interplanetary magnetic field and to magnetospheric substorms. *J. Geophys. Res.* 82 (19), 2723–2734. doi:10.1029/JA082i019p02723

Kan, J. R., and Lee, L. C. (1979). Energy coupling function and solar wind-magnetosphere dynamo. *Geophys. Res. Lett.* 6 (7), 577–580. doi:10.1029/GL006i007p00577

Lockwood, M. (1991). The excitation of ionospheric convection. *J. Atmos. Terr. Phys.* 53 (3), 177–199. doi:10.1016/0021-9169(91)90103-E

Lockwood, M., and Wild, M. N. (1993). On the quasi-periodic nature of magnetopause flux transfer events. *J. Geophys. Res. Space Phys.* 98 (A4), 5935–5940. doi:10.1029/92ja02375

Meng, C. I. (1970). Variation of the magnetopause position with substorm activity. *J. Geophys. Res.* 75 (16), 3252–3254. doi:10.1029/JA075i016p03252

Meng, C. I. (1983). Case studies of the storm time variation of the polar cusp. *J. Geophys. Res. Space Phys.* 88 (A1), 137–149. doi:10.1029/JA088iA01p00137

Newell, P. T., and Meng, C.-I. (1987). Cusp width and B_z: observations and a conceptual model. *J. Geophys. Res. Space Phys.* 92 (A12), 13673–13678. doi:10.1029/JA092iA12p13673

Newell, P. T., Meng, C.-I., Sibeck, D. G., and Lepping, R. (1989). Some low-altitude cusp dependencies on the interplanetary magnetic field. *J. Geophys. Res. Space Phys.* 94 (A7), 8921–8927. doi:10.1029/JA094iA07p08921

Oksavik, K., Moen, J., Carlson, H., Greenwald, R., Milan, S., Lester, M., et al. (2005). Multi-instrument mapping of the small-scale flow dynamics related to a cusp auroral transient. *Ann. Geophys.* 23, 2657–2670. doi:10.5194/angeo-23-2657-2005

Paschmann, G., Haerendel, G., Papamastorakis, I., Sckopke, N., Bame, S. J., Gosling, J. T., et al. (1982). Plasma and magnetic field characteristics of magnetic flux transfer events. *J. Geophys. Res. Space Phys.* 87 (A4), 2159–2168. doi:10.1029/JA087iA04p02159

Pudovkin, M. I., Zaitseva, S. A., Sandholt, P., and Egeland, A. (1996). *Relationship between the cusp aurora poleward motion velocity and solar wind parameters*, 737.

Rijnbeek, R. P., Cowley, S. W. H., Southwood, D. J., and Russell, C. T. (1984). A survey of dayside flux transfer events observed by ISEE 1 and 2 magnetometers. *J. Geophys. Res. Space Phys.* 89 (A2), 786–800. doi:10.1029/JA089iA02p00786

Ross, S. M. (2014). "Chapter 9 - regression," in *Introduction to probability and statistics for engineers and scientists* Editor S. M. Ross Fifth Edition (Boston: Academic Press), 357–444. doi:10.1016/B978-0-12-394811-3.50009-5

Russell, C. T., Chappell, C. R., Montgomery, M. D., Neugebauer, M., and Scarf, F. L. (1971). Ogo 5 observations of the polar cusp on November 1, 1968. *J. Geophys. Res.* 76 (28), 6743–6764. doi:10.1029/JA076i028p06743

Russell, C. T., and Elphic, R. C. (1978). Initial ISEE magnetometer results: magnetopause observations. *Space Sci. Rev.* 22 (6), 681–715. doi:10.1007/bf00212619

Russell, H., and Elphic, R. C. (1979). ISEE observations of flux transfer events at the dayside magnetopause. *Geophys. Res. Lett.* 6 (1), 33–36. doi:10.1029/GL006i001p00033

Sandholt, P. E., Lockwood, M., Oguti, T., Cowley, S. W. H., Freeman, K. S. C., Lybekk, B., et al. (1990). Midday auroral breakup events and related energy and momentum transfer from the magnetosheath. *J. Geophys. Res. Space Phys.* 95 (A2), 1039–1060. doi:10.1029/JA095iA02p01039

Sandholt, P. E., Lybekk, B., Egeland, A., Nakamura, R., and Oguti, T. (1989). Midday auroral breakup. *J. geomagnetism Geoelectr.* 41 (4), 371–387. doi:10.5636/jgg.41.371

Sandholt, P. E., Moen, J., Opsvik, D., Denig, W. F., and Burke, W. J. (1993). Auroral event sequence at the dayside polar cap boundary: signature of time-varying solar wind-magnetosphere-ionosphere coupling. *Adv. Space Res.* 13 (4), 7–15. doi:10.1016/0273-1177(93)90305-U

SandholtDeehr, C. S. A., Egeland, B., Lybekk, R., Romick, G. J., and Viereck, R. (1986). Signatures in the dayside aurora of plasma transfer from the magnetosheath. *J. Geophys. Res. Space Phys.* 91 (A9), 10063–10079. doi:10.1029/JA091iA09p10063

Saunders, M. A., Russell, C. T., and Sckopke, N. (1984). Flux transfer events: scale size and interior structure. *Geophys. Res. Lett.* 11 (2), 131–134. doi:10.1029/GL011i002p00131

Vorobjev, V. G., Gustafsson, G., Starkov, G. V., Feldstein, Y. I., and Shevnina, N. F. (1975). Dynamics of day and night aurora during substorms. *Planet. Space Sci.* 23 (2), 269–278. doi:10.1016/0032-0633(75)90132-4

Xing, Z. Y., Yang, H., Han, D., Wu, Z., Hu, Z., Zhang, Q., et al. (2012). Poleward moving auroral forms (PMAFs) observed at the Yellow River Station: a statistical study of its dependence on the solar wind conditions. *J. Atmos. Solar-Terrestrial Phys.* 86, 25–33. doi:10.1016/j.jastp.2012.06.004

Zhang, L., Wang, C., Wang, J. Y., and Lui, A. (2019). Statistical properties of the IMF clock angle in the solar wind with northward and southward interplanetary magnetic field based on ACE observation from 1998 to 2009: dependence on the temporal scale of the solar wind. *Adv. Space Res.* 63, 3077–3087. doi:10.1016/j.asr.2019.01.023